JACS
JOURNAL OF THE AMERICAN CHEMICAL SOCIETY

Article

A Toolbox Approach to Construct Broadly Applicable Metal-Free Catalysts for Photoredox Chemistry – Deliberate Tuning of Redox Potentials and Importance of Halogens in Donor-Acceptor Cyanoarenes

Elisabeth Speckmeier, Tillmann Fischer, and Kirsten Zeitler

J. Am. Chem. Soc., **Just Accepted Manuscript** • Publication Date (Web): 02 Oct 2018

Just Accepted

ACS Publications

is published by the American Chemical Society. 1155 Sixteenth Street N.W., Washington, DC 20036

A Toolbox Approach to Construct Broadly Applicable Metal-Free Catalysts for Photoredox Chemistry – Deliberate Tuning of Redox Potentials and Importance of Halogens in Donor-Acceptor Cyanoarenes

Elisabeth Speckmeier,[§] Tillmann Fischer[§] and Kirsten Zeitler*

Institut für Organische Chemie, Universität Leipzig, Johannisallee 29, D-04103 Leipzig, Germany.

KEYWORDS: photoredox catalysis, organic dyes, redox potential, donor acceptor molecules, thermally activated delayed fluorescence (TADF)

ABSTRACT: The targeted choice of specific photocatalysts has been shown to play a critical role for the successful realization of challenging photoredox catalytic transformations. Herein, we demonstrate the successful implementation of a rational design strategy for a series of deliberate structural manipulations of cyanoarene-based, purely organic donor-acceptor photocatalysts, using 1,2,3,5-tetrakis(carbazol-9-yl)-4,6-dicyanobenzene (**4CzIPN**) as a starting point. Systematic modifications of both the donor substituents as well as the acceptor´s molecular core allowed us to identify strongly oxidizing as well as strongly reducing catalysts (e.g. for an unprecedented detriflation of unactivated naphthol triflate), which additionally offer remarkably balanced redox potentials with predictable trends. Especially halogen arene core substitutions are instrumental for our targeted alterations of the catalysts´ redox properties. Based on their preeminent electrochemical and photophysical characteristics all novel, purely organic photoredox catalysts were evaluated in three challenging, mechanistically distinct classes of benchmark reactions (either requiring balanced, highly oxidizing or strongly reducing properties) to demonstrate their enormous potential as customizable photocatalysts, that outperform and complement prevailing typical best photocatalysts.

INTRODUCTION

Visible light photoredox catalysis undoubtedly has proven to be a powerful tool for the activation of small molecules, and hence has found widespread applications in a myriad of syntheses and functionalizations to enable formerly challenging or even impossible chemical transformations[1,2,3,4,5] by selective addressing and activation of specific functional groups or bonds. Upon absorption of visible light typical photocatalysts (PCs), either being transition metal-based complexes, or organic dyes, respectively, may reach electronically excited states that enable single electron transfer (SET) and/or energy transfer (ET) to various substrates. Due to their excellent photophysical properties, which have extensively been studied, ruthenium and iridium based photocatalysts[6] are ubiquitously applied as photoredox catalysts and their prominent utility and impressive performance is well established.[1c] However, employment of these precious metal catalysts is associated with elevated costs, and, also in striking contrast to a commitment to sustainability due to their terrestrial scarcity and environmental issues connected with their exploitation.[7] Consequently, broad interest in the development of more sustainable replacement photocatalysts has emerged. Only recently, alternatives based on more earth-abundant first-row transition metals,[8] including Cu,[9] Cr[10] and Fe[11] complexes, have been revisited or newly explored.[12,13]

To address and circumvent the aforementioned limitations and other challenges connected with the use of transition metal complexes (e.g. removing of potential corresponding contaminations from products)[14] the development of purely organic photocatalysts as sustainable and cost-effective alternatives,

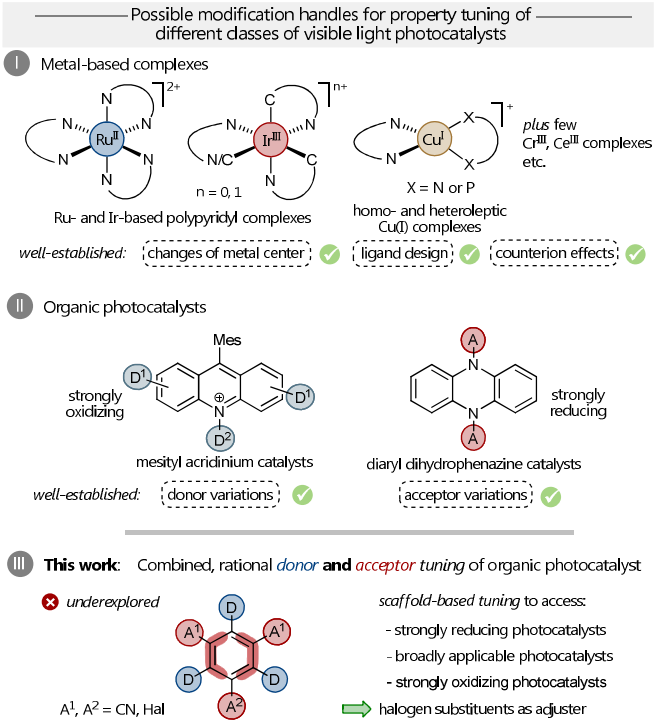

Figure 1. I + II. Compared common approaches for tailoring photocatalysts. III. Conceptual donor & acceptor modifications for accessing both strongly reductive and oxidative properties.

has hence recently attracted enormous interest in the field of photoredox catalysis.[1d,15] While structure-property relationships and the effects of changing metal centers, ligands or counteri-

ons are well-investigated and understood for metal-based complexes (Figure 1/I),[16] comparable investigations to elucidate molecular design principles for organic dyes remain remarkably underexplored.

Despite a rich history and the great potential of organic dyes as photocatalysts[1d,15,17] a conceptually similar treatment as known for transition metal-based complexes, considering the transfer of electron density from electron-rich (metal) centers to electron-deficient positions (ligand) to access charge-transfer excited states (MLCT) and accordingly modify the complex´s redox properties, has not been available for donor-acceptor based organic photocatalysts. Only very recently, structural core modifications in strongly oxidizing acridinium based fluorophores[14,18] were investigated to alleviate their high excited state *oxidation potential* allowing for a more balanced performance in net redox neutral transformations.[14] Similarly, alterations in *N*-aryl substituents of phenothiazines, dihydrophenazines and lately phenoxazines were used to modify their strong *reductive power*. (Figure 1/II)[19]

As recent reports highlight the options to tailor certain organic dye classes for specific catalytic purposes,[18,19,20,21,22] providing *either* strongly *oxidizing or* powerful *reducing* properties, we accordingly questioned whether we could develop tuning guidelines to access broadly applicable, purely organic photocatalysts reaching *both high oxidation* and *reduction potentials* from a single, common scaffold. Prompted by the essential importance of having spatially separated HOMO and LUMO in a non-overlapping frontier molecular orbital (FMO) structure for the construction of thermally activated delayed fluorescence OLED emitters (TADF OLEDs),[23,24] and the initial proof of concept for their photocatalytic activity,[22,23a,] we reasoned the intrinsic charge transfer processes in such TADF materials to be a suitable starting point for our investigations (Figure 1/III).

Building on their favorable photophysical properties, herein, we report a comprehensive study on the deliberate molecular design and modifications of both electron donor and electron acceptor moieties of cyanobenzene derived organic dyes to broadly customize their electrochemical properties and provide insight into their versatile photoredox catalytic activities. Our initial findings for the first time demonstrate the importance of subtle scaffold-based variations, especially with respect to halogen substituents and their previously not considered, ambivalent properties, and hence offer new possibilities to develop tailored organic photocatalysts according to the structure-property relationships established within this study.

RESULTS AND DISCUSSION

General "design" considerations. To identify an appropriate initial dye test system to evaluate the ability of altering the photocatalysts´ electronics and hence tuning their redox properties by modifying core *and* substituents to achieve differences in their charge transfer (CT) characteristics, a number of additional pre-requisites had to be met. For a broadly applicable, competitive performance and to concurrently allow to uncovering direct correlations between structural modifications of the donor-acceptor units and the photocatalyst´s (PC) properties, we aimed at visible light absorbing organic dyes exhibiting sufficient stability. We hence sorted out e. g. acridinium, pyrylium and xanthene derivatives at an early state of our investigations due to their undesirable predisposition for nucleophilic attacks, pH-dependency and ionic character. Apart from accessing longer excited state lifetimes, we centered our efforts on derivatives that could provide a wide redox window allowing for a broad range of both reduction and oxidation processes, referring to the great success and versatile applicability of $Ru(bpy)_3^{2+}$ (also see Figure 5).

While ground state potentials are rather independent of each other and a consequence of the electronic distribution, the simplified mathematical equation for the energy of photoinduced electron transfer[25] directly correlates the excited state potentials to the excited state energy $E_{0,0}$ and the corresponding ground state potential pursuant to the fact that the photocatalyst´s excited state is both a better oxidant and reductant than the PC´s ground state. In other words: within a specific oxidative (or reductive) quenching cycle high ground state potentials lead to low corresponding excited state potentials. As a consequence extremely high ground state redox potentials, such as $E_{1/2}$ (Ir^{III}/Ir^{II}) = –2.19 V *vs* SCE for *fac*-Ir(ppy)$_3$ are barely usable, because the low corresponding excited state potential ($E_{1/2}$ (Ir^{III}*/Ir^{II}) = +0.31 V; $E_{0,0}$ = 2.50 eV) curtails its accessibility.[1c] On the other hand, due to the same interconnection of potentials and $E_{0,0}$, very high excited state potentials, such as $E_{1/2}$ (*Mes-Acr-Me$^+$/Mes-Acr-Me$^\bullet$) = +2.06 V consequently relate to rather low ground state potentials $E_{1/2}$ (Mes-Acr-Me$^+$/Mes-Acr-Me$^\bullet$) = –0.57 V, depending on the respective $E_{0,0}$ energy ($E_{0,0}$ (Mes-Acr-Me$^+$) = 2.63 eV). This may also lead to limitations in applicability, especially within (highly desirable) net redox neutral transformations, where often *both* significant exited state as well as ground state oxidative, resp. reductive power (or *vice versa*) are required to close the catalytic cycle.[14] To better visualize these correlations and their dependency on the excited state energy $E_{0,0}$, we have designed an extended Latimer-type diagram as shown in Figure 2.

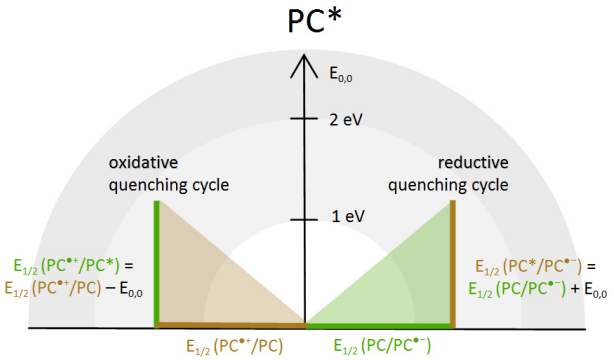

Figure 2. Visualization of ground & excited state (PC*) redox properties of a photocatalyst (PC) in correlation to the corresponding excited state energy $E_{0,0}$ in an *extended Latimer-type diagram*. Different shades of grey correspond to increasing values of $E_{0,0}$ (here: 2.7 eV). Processes of **oxidative** power are marked in golden brown, processes of **reductive** power in green. Oxidative quenching of PC* generates $PC^{\bullet+}$ (left); reductive quenching leads to $PC^{\bullet-}$ (right). For a comparative visualized overview on individual photocatalyst examples and their redox properties using such diagrams, see Figure 5.

For visible light excitation ($\lambda > 400$ nm) the maximum theoretical energy of ≈3.0 eV emphasizes the importance for an almost lossless transformation into excited state energies $E_{0,0}$ to allow for photocatalysts reaching higher, but at the same time still more balanced redox potentials.

Aiming at organic photocatalysts being competitive to current (metal) organic derivatives, we questioned whether thermally activated delayed fluorescence (TADF) emitters (a class of OLED materials[23b,c]) would be ideally suited candidates for structure-property related studies as their inherent characteristics would match our two key requirements for the molecular design of photocatalysts. With the known feature of TADF

materials of small singlet-triplet energy gaps ΔE_{ST}, which can significantly be further decreased by HOMO and LUMO separation in these molecular structures, such donor-acceptor type molecules, including cyanobenzenes, aryl triazines, sulfones and others,[23b,c] should qualify for deliberate structure-correlated design to obtain high oxidation and reduction potentials. Using cyanobenzenes as relatively strong acceptor moieties, we opted to

– combine them with rather weak carbazole and diphenylamine dervatives as corresponding donors and *additionally*

– modify the aromatic acceptor core unit by targeted interchange of the cyano groups with alternative (electron-withdrawing) substituents[26] to thereby

– gain a profound understanding of such unprecedented core modifications and their additional and interconnecting effects on the redox properties of the corresponding catalyst derivatives.

Being aware that these modifications could deteriorate the chemical stability, we planned to then examine and check this issue in corresponding test reactions in comparison to established catalyst systems (see section "*Application and evaluation*").

Selection of building blocks. Founded on Adachi´s most well-known, highly efficient, isophthalonitrile-based green TADF emitter 1,2,3,5-tetrakis(carbazol-9-yl)-4,6-dicyanobenzene (**4CzIPN**)[23a] Zhang and co-workers recently published their efforts to apply a series of positionally interchanged dicyanobenzenes[23a] as donor-acceptor fluorophore-derived photocatalysts.[22] Interestingly, despite the variations of the two cyano groups´ substitution pattern at the benzene core and different numbers of donor carbazoles (Cz), all investigated six carbazolyl dicyanobenzenes (plus one diphenylamine (DPA) derivative) only slightly differed in their redox potentials, but rather showed variations in their stability. Valuing the photocatalysts´ qualification in a decarboxylative photoredox/Ni-catalyzed cross-coupling revealed only minor activity for most derivatives. Nevertheless, **4CzIPN** and **3DPAFIPN**[27] (titled as **4DPAIPN** by Zhang)[28] afforded the products in good yields. Since then, especially **4CzIPN** has successfully been applied as catalyst in a number of different photoredox reactions,[29] most probably due to its balanced redox potential, which proved especially useful for reductive quenching cycles ($(E_{1/2}(PC/PC^{\bullet-}) = -1.24$ V; $E_{1/2}(PC^*/PC^{\bullet-}) = +1.43$ V *vs* SCE; for a full data set, see Table 1 and Figure 5).

Guided by these initial results, we assumed that even higher (ground state) potentials to both sides, oxidation and especially reduction, could be accessible by deliberate structural modifications of these cyanoarene-based donor-acceptor molecules using **4CzIPN** as our starting point. We commenced our photocatalyst design by taking advantage of the "class-inherent" options to both adjust the electronic properties of TADF materials and concomitantly benefit from the extremely small ΔE_{ST} values (between S_1 and T_1: $\Delta E_{ST} < 0.1$ eV; ΔE_{ST} (**4CzIPN**) = 0.08 eV[23a]). Provided by this energetically nearly lossless intersystem crossing (ISC) and reversed intersystem crossing (RISC) processes this would lead to a series of photocatalysts, which are able to transform almost all the absorbed energy of a visible light photon into the excited state, resulting in high excited state energies $E_{0,0}$, and consequently extended redox windows in the excited state. This hence would then allow for both challenging oxidative and reductive quenching cycle processes. With respect to appropriate donor-acceptor combinations and therefore the targeted tunability of the catalysts´ redox potentials, we hypothesized that rational catalyst design should be possible due to the well-known spatial separation of HOMOs, being localized at the donor moieties, and LUMOs distributed over the cyanoarene acceptor core. Sterical hindrance even intensifies this separation of electron-donating aryl amines and the cyanobenzenes as electron acceptor (typical dihedral angle of about 60 ° for **4CzIPN**) allowing (in a first, simplified model) for a nearly independent consideration of reduction and oxidation power by simple, discrete changes at either donor or acceptor part of the photocatalyst PC. The ground state reduction potential $E_{1/2}$ ($PC/PC^{\bullet-}$) is therefore mainly determined by the HOMO of the donor, while the ground state oxidation potential $E_{1/2}$ ($PC^{\bullet+}/PC$) is determined by the LUMO of the acceptor (Figure 3). In addition, electron-donating effects (either by strength or number) should increase the reducing capability of the donor-acceptor system, and inversely LUMO lowering effects should contribute to improved oxidative power.

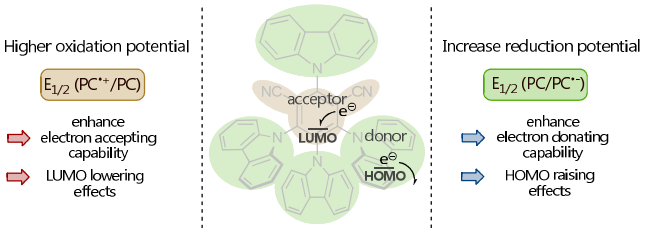

Figure 3. Correlation of redox potentials and influences of donor/acceptor strength and modification.

Following these principles for our catalyst design to set up a series of well-considered donor-acceptor variations of **4CzIPN** as a structural foundation, we chose three donor and five acceptor units (stemming from only three different synthetic precursors) to allow for their correlation to the corresponding redox potentials achieved by the particular donor-acceptor combinations (Figure 4). Our selection of the donor units (3,6-dimethoxy-9*H*-carbazole (**D1**, **MeOCz**), diphenylamine (**D2**, **DPA**) and carbazole (**D3**, **Cz**)) was considered to allow for good comparability of mesomeric, inductive and steric effects as well as the corresponding oxidation potentials as measure for their donor strength.[30]

As our intention was the design of powerful, yet easily accessible organic dyes, we focused on commercially available cyanobenzenes cores as acceptor units,[31] albeit allowing for further acceptor variations by integration of different *halogen substituents* from these precursors, as the virtue of the halogens´ dichotomous character, i. e. having strongly inductive electron withdrawing properties (σ-acceptor), but at the same time mesomeric donating abilities (π-donor character, as well-established in their Hammett σ-factors[32]), seemed to be ideally suited to allow for additional fine-tuning the acceptor properties to alter the overall redox characteristics of the donor-acceptor dyes.[33,34] While the application of fluorine represents an important and mature tool in the design of pharmaceuticals and agrochemicals,[35] fluorine substituents have only been scarcely used in the development of new TADF materials, mainly to blue-shift their emission (higher $E_{0,0}$) or increase the emitters´ solubility.[36] Despite the simplicity of their synthesis from commercially available, inexpensive starting materials, the deliberate core implementation of halogens into donor-acceptor dyes to smoothly *alter their redox properties* (especially with respect to exploit their potential π-donating character) has not yet been realized.[37]

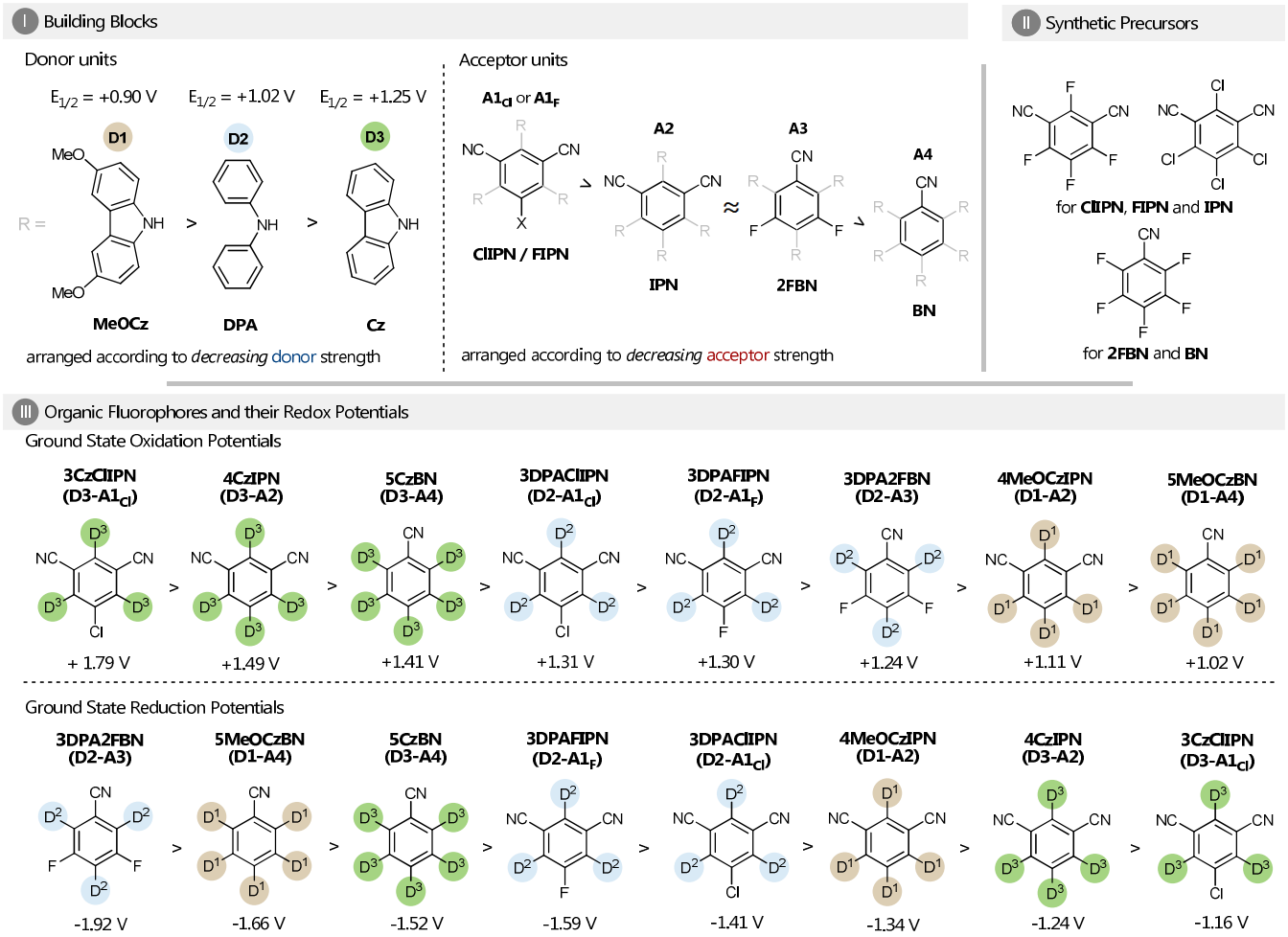

Figure 4. Overview on considered fluorophores, their donor and acceptor units (I) as well as the corresponding synthetic precursors (II). Organic fluorophores are sorted by their *ground state redox potentials* (III). All potentials in Volt *vs* SCE. See supporting information for further details. **D1** : 3,6-dimethoxy-9*H*-carbazole (**MeOCz**); **D2**: diphenylamine (**DPA**); **D3**: carbazole (**Cz**).

In total, we studied eight different organic dyes, thereof three completely new (**3DPAClIPN**, **3DPA2FBN**, **5MeOCzBN**), two of which have only been mentioned in TADF patent literature without any synthesis (**3CzClIPN**, **4MeOCzIPN**),[38] the structurally revised dye **3DPAFIPN** (formerly described as **4DPAIPN**)[22,28] as well as the known fluorophores **4CzIPN**[23a] and **5CzBN**[39] (see Figure 4 for an overview on all catalyst structures). It is important to note that apart from **4CzIPN** (and **3DPAFIPN**[28]) *none* of these organic donor-acceptor molecules has previously been used in any photocatalytic application.

Notably, the synthesis of compounds with more than two *vicinal* diphenylamine groups (e.g. in a combination **D2-A2**) was not possible following the simple one-step nucleophilic substitution S_NAr protocol as published by Adachi[23a] for **4CzIPN** and further used by Zhang[22] for the (misleadingly) reported preparation of alleged **4DPAIPN**.[28,22] The largely increased steric demand caused by the *ortho*-hydrogen atoms of the diphenylamine moieties prevents the synthesis of such **D2**-substituted acceptors exceeding the number of three such entities. Nevertheless, this inherent structural restriction caused by the **DPA** (**D2**) substituent to catalyst structures *without* neighboring **DPA** residues enables the utilization of a simple synthetic protocol to favorably access the corresponding halogen substituted candidates (**D-A1$_{Cl}$**, **D-A1$_{F}$**, **D-A3**).

In order to systematically relate the structural alterations starting from **4CzIPN**, to the corresponding more oxidizing, respectively more reducing ground state redox potentials of our novel photocatalysts, we expected two "effect categories" to be relevant: (1) *donor-based effects*, which would lead to increased reducing power upon rising donor strength and/or number as well as (2) *acceptor-core related modifications* where both number and kind of withdrawing substituents (CN, Cl, F) would matter to increase the oxidation potential. With respect to the special nature of fluorine as σ-acceptor, but π-donor substituent, an additional influence of the core substitution on the reduction potential would be of special interest to reach more exceptional potentials.

Scheme 1 illustrates a series of such stepwise modifications and their particular impact on the redox properties of the corresponding dye.

Discussion and analysis of structure – redox property relationships. A comprehensive survey and analysis of all eight donor-acceptor-type catalysts regarding their ground state oxidation and reduction potential reveals the major principles for the alteration of the corresponding redox potentials. This consequently allows for a predictability of redox properties within our conceptual design approach (see Figure 4). According to a simplified view of the aforementioned HOMO/LUMO separation, an

accepted electron (i. e. reduction of the catalyst ↔ oxidative power) would predominately be localized within the cyanoarene moiety.

The acceptor core´s strong electron withdrawing ability can hence be rationally adjusted by the attached donors (according to their strength) allowing for a significant contribution to further tune the oxidation potential $E_{1/2}$ ($PC^{\bullet+}$/PC). The experimentally determined ground state oxidation potentials (*via* CV measurements) of our accordingly diversified donor-acceptor molecules are in full agreement with this prediction.

Scheme 1. Stepwise alterations of ground state redox potentials for donor-acceptor dyes starting from 4CzIPN.[a]

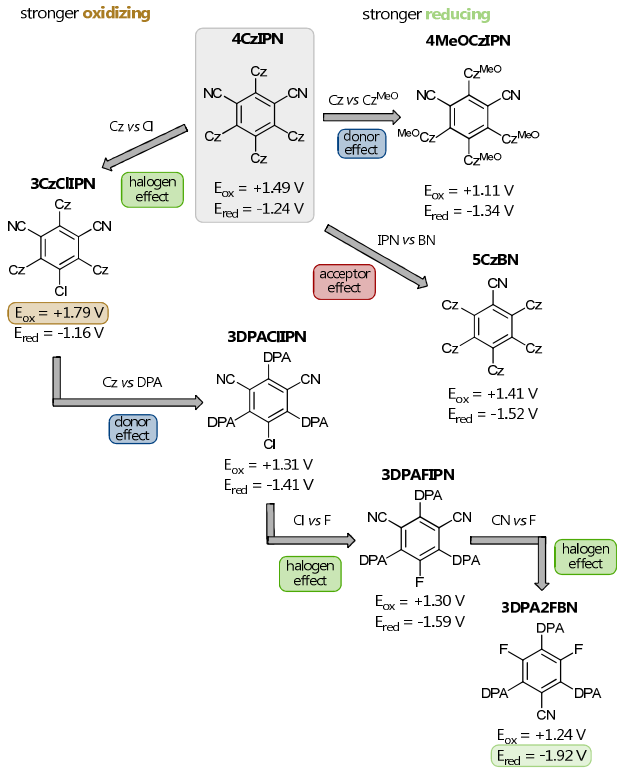

[a] $E_{ox} = E_{1/2}$ ($PC^{\bullet+}$/PC); $E_{red} = E_{1/2}$ (PC/$PC^{\bullet-}$). All values are given in V *vs* SCE.

As expected the combination of the strongest acceptors **ClIPN** with the unsubstituted carbazole **Cz** (**D3**), offering the weakest +M effect (as illustrated by the highest oxidation potential of the free donors ($E_{1/2}$ (ox) = +1.25 V *vs* SCE)), assemble to isophthalonitrile type **3CzClIPN**, reaching the highest ground oxidation potential $E_{1/2}$ ($PC^{\bullet+}$/PC) = +1.79 V *vs* SCE within our series. All investigated catalysts follow a ranking primarily dominated by the strength of the donors' +M effect (*cf.* increasing donor oxidation potential relates to decreasing donor´s +M-effect). Within this classification the ranking then follows the acceptor strength shown in Figure 4/I which of course is intrinsically interconnected with the number of donors contributing to lower the oxidation potential upon their increasing count. Interestingly, interchanging chlorine and fluorine as core substituents at the central benzene ring (**3DPAClIPN** and **3DPAFIPN**) does not display a difference in the observed oxidation potential. Possibly, electron withdrawing inductive effects are counterbalanced by size-dependent mesomeric effects.[32,34]

For our targeted tuning of the reduction potential of these donor-acceptor scaffolds general considerations turned out to be substantially more complicated (notably, most studies correlating electronic effects to redox potentials focus on oxidation potentials[33,34]). Additional to the simple electron donating power of the respective donors (HOMO part of the dye) the consecutive delocalization of the "deficient electron" (i. e. "hole" or positive charge) within the molecule needs to be considered. Due to the missing availability of certain structural patterns a direct comparison to **D2**-substituted dyes mainly fails, while catalysts featuring carbazole donors **D1** and **D3** are well compared according to their structural similarity. The remarkable strongest ground state reducing potential $E_{1/2}$(PC/$PC^{\bullet-}$) = -1.92 V *vs* SCE of **3DPA2FBN** originates from a difluorocyano benzene core in combination with the diphenylamine as strong donor. The rather weak acceptor core may be instrumental to an enhanced delocalization of the "hole" by improved interaction with the π-conjugated donor moieties. Additionally, the twofold fluorine substitution may beneficially contribute to further increase the electron density according to fluorine´s well established electron donating ability (+M). This special fluorine effect becomes more apparent in the direct comparison of the two halogen substituted isophthalonitrile derivatives (**3DPAFIPN** *vs* **3DPAClIPN**) where fluorine clearly increases the reduction power (*cf.* Hammett factors[32]).

Table 1. Excited and ground state redox potentials as well as excited state Energy $E_{0,0}$ of photocatalysts examined.

Photocat	$E_{1/2}$ ($PC^{\bullet+}$/PC*) [V]	$E_{1/2}$ (PC*/$PC^{\bullet-}$) [V]	$E_{1/2}$ ($PC^{\bullet+}$/PC) [V]	$E_{1/2}$ (PC/$PC^{\bullet-}$) [V]	$E_{0,0}$ [eV]
4CzIPN	-1.18	+1.43	+1.49	-1.24	2.67
3DPAFIPN	-1.38	+1.09	+1.30	-1.59	2.68
5CzBN	-1.42	+1.31	+1.41	-1.52	2.83
3DPA2FBN[a]	-1.60	+0.92	+1.24	-1.92	2.84
3CzClIPN	-0.93	+1.56	+1.79	-1.16	2.72
3DPAClIPN	-1.34	+1.24	+1.31	-1.41	2.65
4MeOCzIPN[b]	-1.50	+1.27	+1.11	-1.34	2.61
5MeOCzBN[a]	-1.79	+1.15	+1.02	-1.66	2.81

All potentials in Volt *vs* SCE. Measurements were performed in MeCN unless otherwise noted. [a]Measured in DCM. [b]Measured in MeCN/DCM 5:1 *v/v*.

Considering the structural similar catalysts containing **D1** (**MeOCz**) and **D3** (**Cz**) donors the reduction potentials then follow a logical ranking referring to the overall donation power of the system. **MeOCz** as better electron donor, according to its stronger, 5-methoxy-group induced +M-effect, outranges the corresponding **Cz** substituted derivatives by reductive power. Apart from this, stronger acceptors (as judged by the electron-withdrawing cyano and chlorine substituents of the arene core) display their inferior ability to contribute to the delocalization of the "hole" and hence determine the overall ranking of the ground state reduction potentials. Notably, within the series of examined organic dyes seemingly small structural changes allow to access largely different redox potentials (see Table 1). Our deliberate structural modifications of the parent cyanoarene scaffold led to a considerable bandwidth of Δ($\Delta E_{1/2}$ (PC/$PC^{\bullet-}$)) = 0.76 V and Δ($\Delta E_{1/2}$ (PC*/$PC^{\bullet-}$) = 0.64 V) of the reductive quenching side and Δ($\Delta E_{1/2}$ ($PC^{\bullet+}$/PC)) = 0.77 V and Δ($\Delta E_{1/2}$ ($PC^{\bullet+}$/PC*)) = 0.86 V for oxidative quenching.

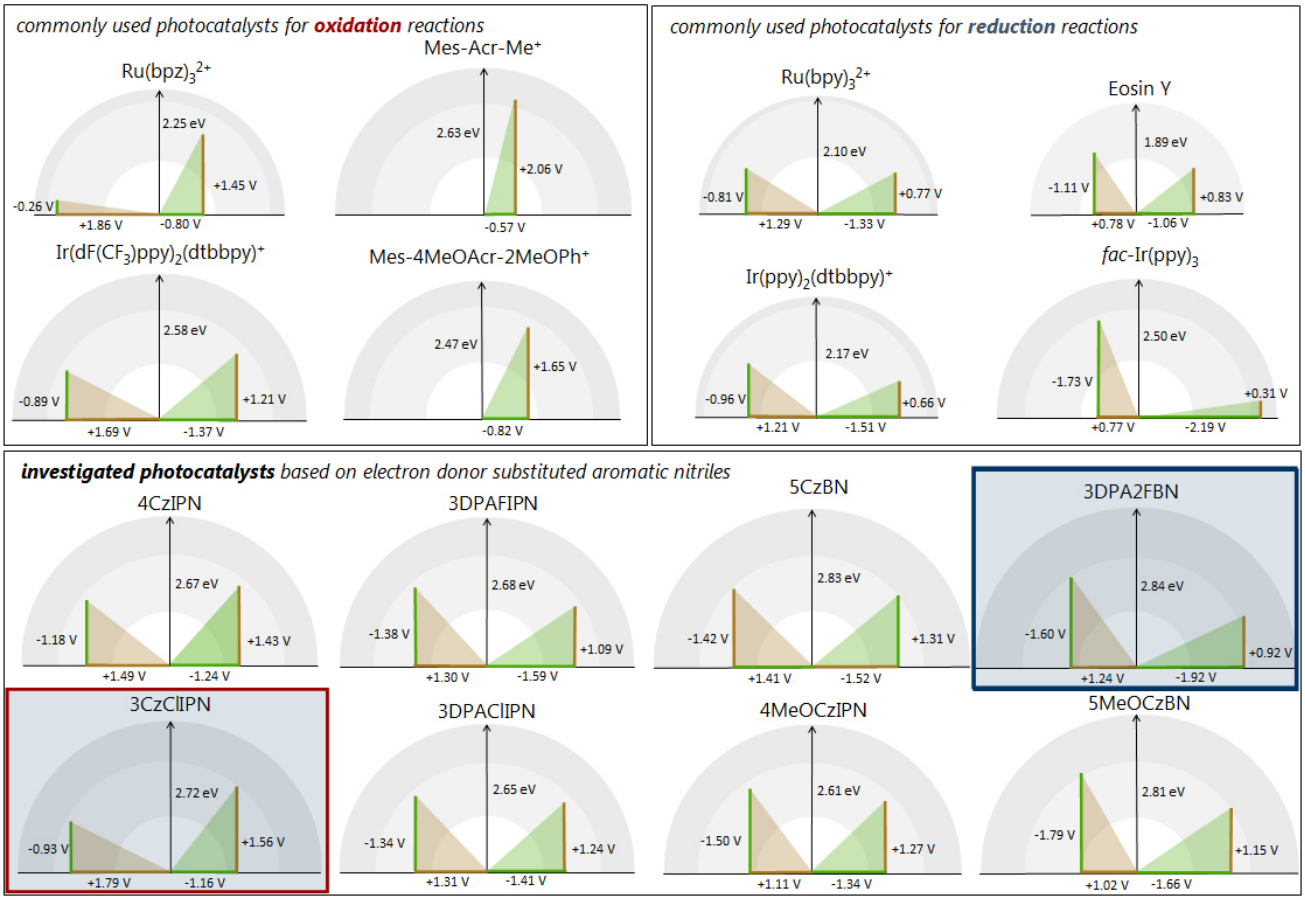

Figure 5. Overview of common visible light photocatalysts and all investigated photocatalysts in this study, displaying their redox potentials *vs* SCE[40] plus $E_{0,0}$ energies in extended Latimer-type diagrams.

Remarkably, the excited state energies $E_{0,0}$ also clearly exceed the range as observed for **4CzIPN**. With our structural alterations significantly higher $E_{0,0}$ values up to 2.84 V could be observed (**3DPA2FBN** – as triggered by the fluorine substituents[36]). These high $E_{0,0}$ values offer, besides the high ground state redox potentials $E_{1/2}$ ($PC/PC^{\bullet-}$) and $E_{1/2}$ ($PC^{\bullet+}/PC$) as function of the donor-acceptor properties, additionally strong excited state redox potentials $E_{1/2}$ ($PC^{\bullet+}/PC^*$) and $E_{1/2}$ ($PC^*/PC^{\bullet-}$). Such an equal distribution of redox potentials so far was only available for transition metal based[40] complexes such as for $Ir(ppy)_2(dtbpy)^+$, $Ir(dF\text{-}CF_3\text{-}ppy)_2(dtbpy)^+$ and $Ru(bpy)_3^{2+}$ (*cf.* Figure 5), albeit with considerably lower absolute values. Comparison of the redox properties of the current, most common photocatalysts with our newly designed organic dyes (Figure 5), clearly reveals the advantage of our donor-acceptor photocatalysts both with respect to their remarkable redox properties, but additionally regarding to the balanced distribution of reductive and oxidative power. The predictable tunability combined with these extended, balanced redox windows provides a broad range of novel photocatalysts of versatile usability to outperform and largely complement current best-practice photocatalysts for both oxidative and reductive applications.

Application and evaluation of photocatalytic performance. Having established promising structure-property relationships for our donor-acceptor dyes, we aimed to challenge the newly designed family of photocatalysts in suitable test reactions to probe and highlight their stability and specific reactivity in both common oxidative and reductive transformations. While all eight photocatalysts should be capable of catalyzing a broad range of reactions due to their large, yet balanced redox windows (*cf.* Figure 5), we focused for their evaluation on challenging reactions either requiring strongly oxidative or highly reductive power, as well as such in need of counterbalanced potentials (e.g. for net redox neutral transformations). To evaluate and compare the photocatalysts´ performance according to their customized redox properties, we therefore selected four mechanistically distinct reactions.

(1) *Decarboxylative, Giese-type conjugate addition.*

The photocatalytic, decarboxylative conjugate addition of *N*-protected amino acids to electron-poor olefins was initially investigated by MacMillan and co-workers using $Ir(dF(CF_3)ppy)_2(dtbpy)^+$ as best-performing catalyst.[41] This transformation does not only strongly rely on the (exited state) oxidative power of the photocatalyst to mediate the decarboxylation process (*cf.* e. g. Boc-Pro-OCs, $E_{1/2}$ (red) = +0.95 V *vs* SCE) – notably, a dramatic decrease of product yields was observed if employing less oxidizing Ir-complexes – but also subsequently requires sufficient reducing potential to then yield the corresponding enolate by SET reduction of the *in situ* generated α-acyl radical (*cf.* $E_{1/2}$ (red) = –0.60 V *vs* SCE).[41] Hence, this C-C cross coupling reaction was already successfully applied as test reaction for acridinium based

photocatalysts by DiRocco and Nicewicz[14] and turned out to be highly suitable to carve out the catalysts´ distinct differences. We investigated the performance of our photocatalysts in comparison to the formerly best acridinium catalyst as identified by DiRocco.[14]

Table 2: Photocatalytic decarboxylative conjugate addition of Cbz-proline to diethyl maleate.

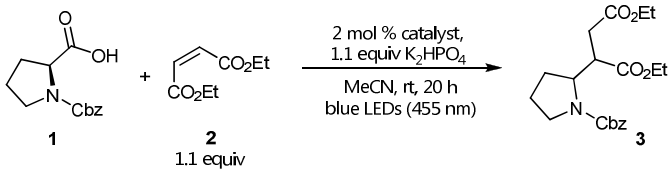

entry[a]	photocatalyst	yield[b] of **3**
1	**4CzIPN**	80%[c]
2	**3DPAFIPN**	16%
3	**5CzBN**	37%
4	**3DPA2FBN**	20%
5	**3CzClIPN**	77%[c]
6	**3DPAClIPN**	12%
7	**4MeOCzIPN**	3%
8	**5MeOCzBN**	1%
9	**Mes-4MeOAcr-2MeOPh$^+$**	73%[c,d]

Formerly *best catalyst* for this decarboxylative redox-neutral transformation

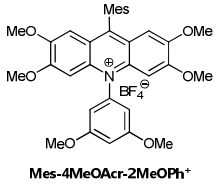

Mes-4MeOAcr-2MeOPh$^+$

[a] conditions: Cbz-Pro-H (**1**) (0.20 mmol), diethyl maleate **2** (0.22 mmol), photocatalyst (2.0 mol %), K_2HPO_4 (0.22 mmol), MeCN (4 mL), irradiation with blue LEDs at rt. [b] yield determined by GC-FID using mesitylene as internal standard. [c] yield of isolated product. [d] according to ref. 14: yield 86% as calculated *via* HPLC assay.

With excited state potentials $E_{1/2}$ (PC*/PC$^{\bullet-}$) from +1.56 V (**3CzClIPN**) to +0.92 V (**3DPA2FBN**) and corresponding ground state reduction potentials in the range of $E_{1/2}$ (PC/PC$^{\bullet-}$) from –1.92 V (**3DPA2FBN**) to –1.16 V (**3CzClIPN**) *vs* SCE (reductive quenching cycle) most of our catalysts should engage in a SET oxidation of the carboxylate formed by deprotonation of Cbz-proline (**1**), radical addition to diethylmaleate (**2**) and the subsequent reduction to close the net redox neutral catalytic cycle. Our best oxidizing candidates **3CzClIPN** (77%) and **4CzIPN** (80%) were monitored to afford even higher yields of addition product **3** than DiRocco´s best candidate **Mes-4MeOAcr-Ph$^+$**.[14]

In good agreement with the results of MacMillan[41] other candidates with less oxidation power were also able to perform the reaction, albeit with considerably lower yields (12-37%, entries 2-4,6). Despite their fitting excited state oxidation potentials (Figure 5 and Table 1), the two **MeOCz**-substituted dye derivatives only could barely generate product **3** (entries 7 and 8). We asssume that these both catalysts (**4MeOCzIPN** and **5MeOCzBN**) perform a fast intramolecular, unproductive (back) electron transfer from their excited CT state, and hence by such an internal quenching may prevent their engagement in productive catalytic cycles.[42]

(2) *Oxidative photocatalytic bromination of arenes*.

Considering the favorable oxidative properties of our catalyst **3CzClIPN**, we were interested to further explore even more challenging oxidative transformations in order to assess its operating scope. We hence additionally examined the photocatalytic bromination of anisole, originally developed by Fukuzumi and co-workers.[43] Formerly this reaction, which requires the initial, rather demanding oxidation of anisole to its arene radical cation ($E_{1/2}$ (MeOAr/MeOAr$^{\bullet+}$) = +1.79 V *vs* SCE) could only be conducted using powerful oxidative photocatalysts, such as *Fukuzumi´s catalyst* **Mes-Acr-Me$^+$** (for redox data, see Figure 5). Gratifyingly, **3CzClIPN** could equally perform this challenging reaction following the reference conditions (Table 3).

Table 3: Photocatalytic bromination of anisole.

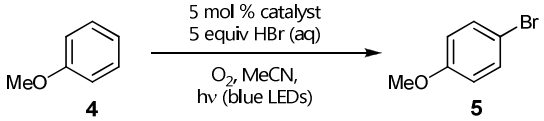

entry	catalyst	reaction time[b]	yield[c] of **5**
1	**Mes-Acr-Me$^+$**	16 h	87%
2	**3CzClIPN**	16 h	89%

[a] irradiation with blue LEDs. b yield determined by GC-FID using mesitylene as internal standard.

As the excited state oxidation potential of **3CzClIPN** ($E_{1/2}$ (PC*/PC$^{\bullet-}$) = +1.56 V *vs* SCE) might be slightly too low to operate the reaction, as mainly referred, following a reductive quenching cycle, an oxidative quenching cycle accessing the better fitting catalyst´s ground state oxidation potential ($E_{1/2}$(PC$^{\bullet+}$/PC) = +1.79 V *vs* SCE) by initial reduction of molecular oxygen could be considered (Scheme 3). This alternative mechanistic option again clearly points to the intrinsic advantages of photocatalysts with well-balanced redox potentials.

Scheme 2. Comparison of both possible quenching cycles for the mechanism of oxidative arene bromination.

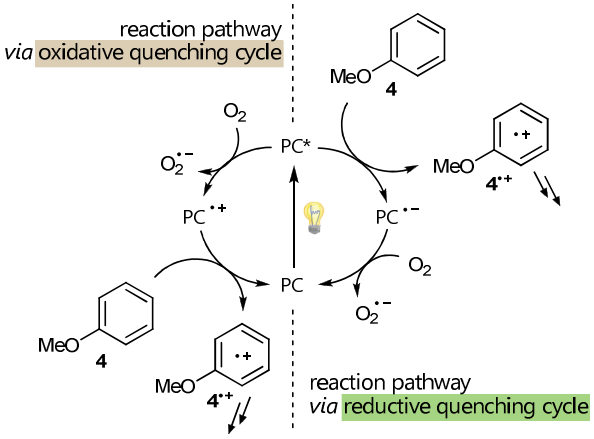

(3) *Photocatalytic, dual carbonyl reduction reactions for sequential C-O bond activation based C-C bond formation.*

To assess the reductive performance of our catalyst series we selected the reductive C-O bond cleavage reaction of a lignin model derivative (**6**) as a benchmark reaction. While this transformation developed by Stephenson and co-workers[44] had already been accordingly used for the photocatalytic evaluation of a 4CzIPN-derived carbazolic porous organic framework,[45] we considered this reaction to be an especially favorable, yet challenging test system for additional reasons.

Based on the similarity of conditions of Stephenson[44] to such as published by Rueping for a reductive pinacol-type coupling of acetophenone derivatives,[46] we hypothesized that the generated product *p*-methoxy acetophenone (**7**) would hold the option for a second, even more challenging reduction process to be possible, subject to the stability and efficiency of the catalysts employed. This would allow for a unprecedented sequential combination of two different, consecutive reductions by a single photocatalyst (Scheme 3).

Scheme 3. A sequential, double photocatalytic reduction strategy for the transformation of lignin derivatives (cycle I) to pinacols (cycle II).[a]

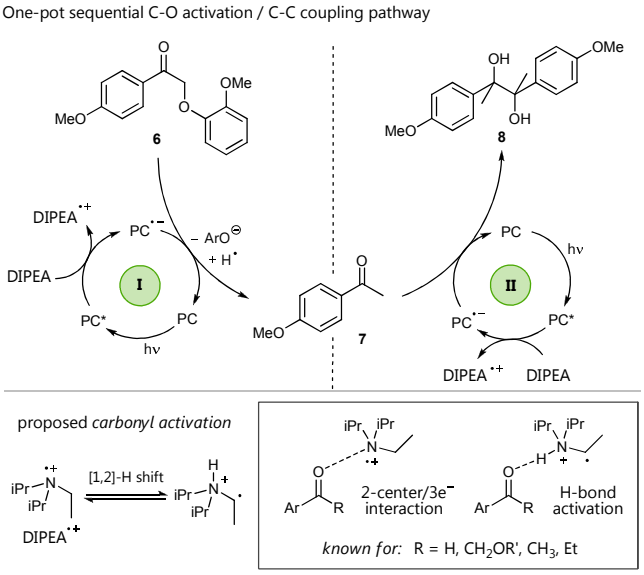

[a] Cycle **I**: C–O bond cleavage. Cycle **II**: ketyl radical-promoted homocoupling (pinacol formation).

Relying on the differing requirements for the two sequential transformations, we hoped to use this system to single out the specific differences in the catalytic performance of our catalysts. To evaluate the reductive power of the catalyst series we initially followed reaction conditions of Stephenson (irradiation time: 12 h).[44] However, we were not able to obtain the expected acetophenone product **7** in high yields. In fact, pinacol **8** was isolated as main product in most cases (Table 4). In an additional control reaction we also predominantely obtained the pinacol product **8** in 56% yield with Stephensons` originally applied catalyst $Ir(ppy)_2(dtbbpy)(PF_6)$ (entry 9). This hence points to the supposed, subsequent coupling reaction of the product of the initial C-O bond cleavage after 12 h of irradiation,[47] being in in good agreement with the pinacol reaction published by Rueping[46] employing similar conditions. Notably, the reductive C–O bond cleavage of lignin model derivative **6** (Table 4) was achieved in *quantitative* yields with all tested catalysts, except for eosin Y (Table 4, entry 10) used in a control reaction. To account for a more detailed analysis of the reductive properties of our catalysts, we therefore additionally monitored the irradiation time to reach full conversion of starting material **6** to acetophenone **7** and further recorded the yield of pinacol **8** (determined by isolation) in the second, more demanding reduction. Here we could observe significant difference for the time to reach full conversion of compound **6**.

Table 4. Sequential C–O-bond cleavage with subsequent reductive pinacol coupling.

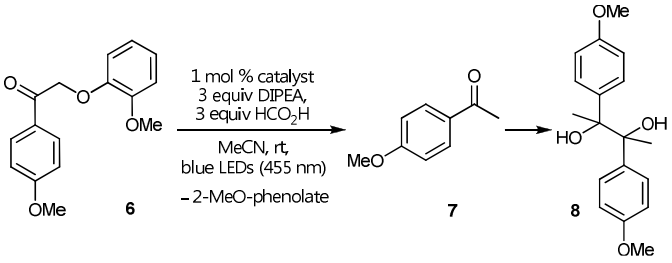

entry[a]	photocatalyst	time to full conversion of **6**[b]	yield[c] of **8**
1	**4CzIPN**	3 h	61%
2	**3DPAFIPN**	1 h	64%
3	**5CzBN**	1 h	69%
4	**3DPA2FBN**	2 h	77%
5	**3CzClIPN**	3 h	0%
6	**3DPAClIPN**	45 min	64%
7	**4MeOCzIPN**	5 h	0%
8	**5MeOCzBN**	5 h	0%
9	$[Ir(ppy)_2(dtbbpy)](PF_6)$	1 h	56%[d]
10	Eosin Y	-[e]	0%

[a] conditions: **6** (0.5 mmol), DIPEA (1.5 mmol), HCO_2H (1.5 mmol), photocatalyst (1 mol %), MeCN (2.5 mL), irradiation with blue LEDs. [b] conversion of **6** and yield of **7** monitored by GC-FID with mesitylene as internal standard. [c] isolated yield after 18 h of irradiation. [d] 12 h of irradiation (*cf.* ref. 44). [e] after 24 h only traces of acetophenone **7** could be detected.

With respect to the required redox properties for these transformations the initial C–O bond cleavage may only be reached by high reductive potentials (*cf.* e.g. $E_{1/2}$ (red) = –1.74 V *vs* SCE for 2-oxo-2-phenylethyl acetate) while the subsequent pinacol formation is even more challenging (*cf.* e.g. acetophenone, $E_{1/2}$ (red) = –2.64 V *vs* SCE[46]). The large deviation compared to the reduction potentials available for our catalyst family (table 1, Figure 4 and 5) suggests an additional LUMO-lowering activation of the carbonyl group to be operative. DIPEA as tertiary amine may not only act as a sacrificial electron donor in this reaction sequence and HAT donor in cycle **I** (*cf.* scheme 3), but also may considerably contribute to an additional activation of the carbonyl group *via* H-bond interaction, respectively a related LUMO-lowering 2-center/3-e$^-$ interaction (Scheme 3, lower part) as suggested by Rueping.[46] This requirement for additional LUMO activation is in good agreement with our previous work, where related reductive C–O-bond cleavage reactions also required either DIPEA, ascorbic acid, or Lewis

acids. respectively, as an additional activation tool.[48] Such a dual catalytic,[3] synergistic activation would also well explain the discrepancy in the reduction potential of the weaker catalysts and the required potential to mediate the C–O bond breakage.

Taking hence the more demanding subsequent pinacol coupling as a benchmark test for the reductive properties of the donor-acceptor photocatalysts, we could well match the observed performance with their redox potentials. For nearly all catalysts the pinacol product **8** was obtained in good yields (61-77%; isolated yield of the two-step process), except for **3CzClIPN** (Table 4, entry 5), owing the lowest reduction potential ($E_{1/2}(PC/PC^{\bullet-}) = -1.16$ V *vs* SCE), and the methoxy-carbazole substituted candidates **4MeOCzIPN** and **5MeOCzBN**. Despite being unserviceable to mediate the pinacol coupling (and the oxidative decarboxylation as shown before (Table 2)), these two MeOCz-substituted catalysts were still able to catalyze the initial C–O bond cleavage, however by slower rate. **3DPA2FBN**, displaying the highest reduction potential ($E_{1/2}(PC/PC^{\bullet-})$ = –1.92 V *vs* SCE), in contrast allowed for fast transformation providing the highest observed yield (entry 4).

(4) *Photocatalytic, reductive detriflation of arene triflates.*

With respect to the impressive reductive properties as determined for catalyst **3DPA2FBN**, we finally set out to investigate its performance in a highly challenging detriflation of unactivated aryl triflates (typical range of $E_{1/2}$ (red): –2.65 V to –1.95 V *vs* SCE).[49]

Importantly, the photocatalytic defunctionalization of such non-activated substrates has previously not been described as even stronger reducing potentials are required; related photoredox catalytic transformations could by now only be achieved employing activated aryl triflates (e.g. *p*-CN-benzene derivatives).[50] Current best-performing, visible light photocatalytic reduction methods try to bypass the above mentioned photophysical restrictions (in terms of providing E > 3.0 eV). Among the recently reported, highly successful concepts in this context are procedures relying on consecutive electron-transfer approaches such as *con*PET either employing perylene bisimides (PDIs)[51] or rhodamine-6G (**Rh-6G**) as photocatalyst.[52] Other very powerful "super-reducing" photocatalytic methods like *SenI*-ET (sensitization-initiated electron transfer) using a combination of $Ru(bpy)_3Cl_2$ and aromatic hydrocarbons such as pyrene,[50a] or TTA (triplet-triplet annihilation)[53] build on a favorable combination of energy transfer processes together with successive electron transfers. All these procedures provide unique, novel opportunities to address transformations that require extremely high reductive power.

To finally compare the reductive power of our best reducing catalyst **3DPA2FBN** ($E_{1/2}(PC/PC^{\bullet-})$ = –1.92 V *vs* SCE) to such protocols, we chose the simple, but challenging defunctionalization of naphthol triflate **9**, whose detriflation would require high reduction potentials ($E_{1/2}$ (red) = –2.01 V *vs* SCE for **9**).[49]

Surprisingly, using **3DPA2FBN** and also strongly reductive metal-complex based photocatalyst *fac*-$Ir(ppy)_3$, we were able to achieve remarkably better results in the reduction of our non-activated aromatic triflate than upon application of the aforementioned *SenI*-ET and *con*PET strategies (Table 5, entries 6 and 7).

Table 5: Detriflation of 2-naphthol triflate (9).

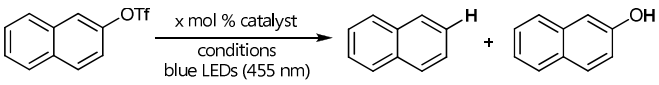

9 10 11

entry	photocatalyst	conditions	reaction time[b]	yield[b] of **10** | **11**
1	**3DPA2FBN** 1 mol % c(PC) = 2 mM	3 equiv DIPEA 3 equiv HCO_2H MeCN	8 h	21% | 60% **Σ 81%**
2	*fac*-$Ir(ppy)_3$ 1 mol % c(PC) = 2 mM	3 equiv DIPEA 3 equiv HCO_2H MeCN	8 h	22% | 59% **Σ 81%**
3	**3DPA2FBN** 1 mol % c(PC) = 0.4 mM	3 equiv DIPEA 3 equiv HCO_2H MeCN	12 h	23% | 63% **Σ 86%**
4	*fac*-$Ir(ppy)_3$ 1 mol % c(PC) = 0.4 mM	3 equiv DIPEA 3 equiv HCO_2H MeCN	8 h	26% | 64% **Σ 90%**
5	**3DPA2FBN** 2 mol % c(PC) = 4 mM	3 equiv DIPEA 3 equiv HCO_2H MeCN	6 h 8 h	23% | 65% **Σ 88%** 24% | 67% **Σ 91%**
6	**Rh-6G** 10 mol %	2.2 equiv DIPEA DMSO degassed	24 h	0% | 0% **Σ 0%**
7	$[Ru(bpy)_3]Cl_2$ 1 mol %, pyrene 5 mol %	1.4 equiv DIPEA DMSO degassed	12 h	8% | 34% **Σ 42%**

[a] irradiation with blue LEDs. [b] determined by GC-FID with mesitylene as internal standard.

While the selectivity of the bond-cleavage (C-O *vs* S-O) upon SET to the triflate is the same for all investigated strategies (according to the common SET-initiated mechanism), both the overall yield of products **10** and **11** resulting from the initial reduction step as well as the reaction time differ considerably.[54]

Starting with typical conditions following a reductive quenching cycle **3DPA2FBN** demonstrates its remarkable reductive power with a total yield of 81% after 8 h of irradiation (table 5, entry 1). Only *fac*-$Ir(ppy)_3$ as commonly used, strongly reductive precious metal-based catalyst could afford the same overall yield of **10+11** (entry 2). *SenI*-ET conditions only provided 42% yield after 12 h (entry 7), while the in other respects highly successful alternative *con*PET strategy completely failed to perform this reduction (entry 6); even after 24 h irradiation no conversion of the starting material could be observed.

With respect to the clearly limited solubility of *fac*-$Ir(ppy)_3$ in acetonitrile, we additionally evaluated the differences in performance for the two best catalysts in this transformation according to altering catalyst molarities. Changing from c(photocat) = 2 mM (equivalent to c(substrate **9**) = 0.2 M) to a catalyst concentration of c(photocat) = 0.4 mM *fac*-$Ir(ppy)_3$ shows improved conversion under these highly diluted conditions (entry 4), while this lower concentration lengthens the time for **3DPA2FBN** to reach full conversion (entry 3).

Importantly, a high overall yield can still be obtained (86% after 12 h), pointing to a sound catalyst stability. Doubling the loading of photocatalyst **3DPA2FBN** within the more concentrated reaction set-up[55] (entry 5) leads to a significant acceleration providing high yields of around 90% only after 6 h reaction time. As demonstrated for this unprecedented aryl detriflation the consideration of further aspects relevant to the actual attractiveness of a process, such as costs, handling or scale-up issues etc., clearly reveals obvious advantages for our novel, strongly reducing organic photocatalyst **3DPA2FBN** as compared to other catalyts or strategies.

CONCLUSION AND OUTLOOK

In summary, we have synthesized and studied eight donor-acceptor molecules (including five completely new photocatalysts) to elucidate their structure-property relationships, which we could beneficially use for targeted structural modification to obtain remarkably high specific redox potentials based on deliberate structural changes. Installation of halogen substitutions at the arene core were crucial to reach the most highly reducing and the most highly oxidizing catalysts (Figure 6).

All catalysts stand out due to their balanced redox potentials and their therefore broad applicability in concert with a sound chemical stability. Moreover, we extensively evaluated all our organic photocatalyst candidates in different challenging oxidative and reductive photocatalytic transformations in comparison to current best-practice catalysts.

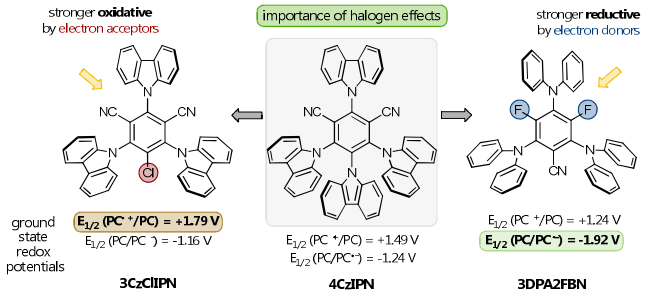

Figure 6. Structures and properties of our balanced, most oxidizing (**3CzClIPN**) and reducing photocatalysts (**3DPA2FBN**) in comparison to **4CzIPN**.

Owing to their extended redox windows we could identify photocatalysts for all benchmark reactions, which clearly can successfully compete with the hitherto known best catalysts for the respective reactions, while offering the additional advantage of being easily accessible, inexpensive and metal-free. Lastly, we could demonstrate the unprecedented photocatalytic reduction of a non-activated aryl triflate.

The sustained need for abundant and reasonably priced, non-metal photocatalysts makes our new family of donor-acceptor dyes a highly attractive alternative to commonly used Ru- and Ir-based catalysts. Based on their wide redox windows and their expedient stability as demonstrated in a broad range of benchmark reactions, we expect these organic photocatalysts to be broadly applicable for developing new photoredox catalyzed, synthetic methodologies.

ASSOCIATED CONTENT

Supporting Information. Experimental procedures and characterization data for all compounds, including copies of ^{1}H NMR, ^{13}C NMR, ^{19}F NMR (PDF), HR MS spectra, cyclic voltammetry, absorption and emission spectra, lifetime decay curves.

This material is available free of charge via the Internet at http://pubs.acs.org.

AUTHOR INFORMATION

Corresponding Author

*E-mail: kzeitler@uni-leipzig.de

ORCID

Kirsten Zeitler: 0000-0003-1549-5002

Author Contributions

§ These authors contributed equally.

Notes

The authors declare no competing financial interest.

Funding Sources

This work was generously supported by the Deutsche Forschungsgemeinschaft (DFG, GRK 1626).

ACKNOWLEDGMENT

We thank Regina Hoheisel (University of Regensburg) for her assistance with cyclic voltammetry, M. Sc. Simon Pfeiffer (University of Leipzig) for his assistance with absorbance, emission and lifetime measurements and Dr. Lothar Hennig (University of Leipzig) for his support in terms of the structure determination *via* NMR.

ABBREVIATIONS

General (selected). **A**: acceptor; *con*PET: consecutive photoinduced electron transfer; CT: charge transfer; **D**: donor; ET: energy transfer; HAT: hydrogen atom transfer; ISC: intersystem crossing; MLCT: metal-to-ligand chargetransfer; OLED: organic light emitting diode; PC: photocatalyst; ppy: 2-phenylpyridine; RSIC: reversed intersystem crosssing; *SenI*-ET: sensitization-initiated electron transfer; SET: single electron transfer; TADF: thermally activated delayed fluorescence; TTA: triplet-triplet annihilation;

Names and Nomenclature. **BN**: benzonitrile (**A4**); **ClIPN**: 5-chloro *iso*phthalonitrile (**A1$_{Cl}$**); **Cz**: carbazole (**D3**); **DPA**: diphenylamine (**D2**); **2FBN**: 3,5-difluoro benzonitrile = *meta,meta´*-difluoro benzonitrile (**A3**); **FIPN**: 5-fluoro *iso*phthalonitrile (**A1$_{F}$**); **IPN**: isophthalonitrile (**A2**); **MeOCz**: 3,6-dimethoxy-9*H*-carbazole (**D1**); **Mes-Acr-Me^{+}**: 9-Mesityl-10-methylacridinium; **PDI**: perylene bisimide; **Rh-6-G**: rhodamine-6G.

REFERENCES

(1) Selected reviews: (a) Zeitler, K. Photoredox Catalysis with Visible Light. *Angew. Chem., Int. Ed.* **2009**, *48*, 9785–9789. (b) Special issue "Photoredox Catalysis in Organic Chemistry": *Acc. Chem. Res.* **2016**, *49*. (c) Prier, C. K.; Rankic, D. A.; MacMillan, D. W. C. Visible Light Photoredox Catalysis with Transition Metal Complexes: Applications in Organic Synthesis. *Chem. Rev.* **2013**, *113*, 5322–5363. (d) Romero, N. A.; Nicewicz, D. A. Organic Photoredox Catalysis. *Chem. Rev.* **2016**, *116*, 10075–10166. (e) Ravelli, D.; Protti, S.; Fagnoni, M. Carbon–Carbon Bond Forming Reactions *via* Photogenerated Intermediates. *Chem. Rev.* **2016**, *116*, 9850–9913. (f) Marzo, L.; Pagire, S. K.;

Reiser, O.; König. B. Visible - Light Photocatalysis: Does it make a difference in Organic Synthesis? *Angew. Chem., Int. Ed*. **2018**, *57*, 10034–10072.

(2) Selected recent books: (a) *Chemical Photocatalysis*; König, B., Ed.; deGruyter: Berlin, 2013. (b) *Visible Light Photocatalysis in Organic Chemistry*; Stephenson, C. R. J.; Yoon, T. P.; MacMillan, D. W. C., Eds.; Wiley-VCH: Weinheim, 2018.

(3) For recent reviews covering dual activation photocatalysis, see: (a) Neumann, M; Zeitler, K. Synergistic Visible Light Photoredox Catalysis. In *Chemical Photocatalysis*; König, B., Ed.; deGruyter: Berlin, 2013; p. 151. (b) Hopkinson, M. N.; Sahoo, B.; Li, J.-L.; Glorius, F. Dual Catalysis See the Light: Combining Photoredox with Organo-, Acid, and Transition-Metal Catalysis. *Chem. Eur. J.* **2014**, *20*, 3874–3886. (c) Skubi, K. L.; Blum, T. R.; Yoon; T. P. Dual Catalysis Strategies in Photochemical Synthesis. *Chem. Rev.* **2016**, *116*, 10035–10074. (d) Twilton, J.; Le, C. C.; Zhang, P.; Shaw, M. H.; Evans, R. W.; MacMillan, D. W. C. The Merger of Transition Metal and Photocatalysis. *Nat. Rev. Chem.* **2017**, *1*, 0052.

(4) (a) DiRocco, D. A.; Dykstra, K.; Krska, S.; Vachal, P.; Conway, D. V.; Tudge, M. Late–Stage Functionalization of Biologically Active Heterocycles Through Photoredox Catalysis. *Angew. Chem., Int. Ed.* **2014**, *53*, 4802–4806. (b) Cernak, T.; Dykstra, K. D.; Tyagarajan, S.; Vachal, P.; Krska, S. W. The Medicinal Chemist's Toolbox for Late Stage Functionalization of Drug-Like Molecules. *Chem. Soc. Rev.* **2016**, *45*, 546–576.

(5) Selected reviews: (a) Corrigan, N.; Shanmugam, S.; Xu, J.; Boyer, C. Photocatalysis in Organic and Polymer Synthesis, *Chem. Soc. Rev*. **2016**, *45*, 6165–6212. (b) Michaudel, Q.; Kottisch, V.; Fors, B. P. Cationic Polymerization: From Photoinitiation to Photocontrol. *Angew. Chem., Int. Ed.* **2017**, *56*, 9670–9679. (c) Chen, M.; Zhong, M.; Johnson, J. A. Light-Controlled Radical Polymerization: Mechanisms, Methods, and Applications, *Chem. Rev.* **2016**, *116*, 10167–10211.

(6) (a) Juris, A.; Balzani, V.; Barigelletti, F.; Campagna, S.; Belser, P. von Zelewsky, A. Ru(II) Polypyridine Complexes: Photophysics, Photochemistry, Electrochemistry, and Chemiluminescence. *Coord. Chem. Rev.* **1988**, *84*, 85–277. (b) Tucker, J. W.; Stephenson, C. R. J. *J. Org. Chem*. **2012**, *77*, 1617–1622. (c) Teegardin, K.; Day, J. I.; Chan, J.; Weaver, J. Advances in Photocatalysis: A Microreview of Visible Light Mediated Ruthenium and Iridium Catalyzed Organic Transformations. *Org. Process Res. Dev.* **2016**, *20*, 1156– 1163. (d) Monos, T. M.; Stephenson, C. R. J. Photoredox Catalysis of Iridium(III) - Based Photosensitizers. In *Iridium(III) in Optoelectronic and Photonics Applications;* Zysman-Colman, E., Ed.; Wiley & Sons: Chichester, 2017; p. 541.

(7) (a) Volz, D.; Wallesch, M.; Fléchon, C.; Danz, M.; Verma, A.; Navarro, J. M.; Zink, D. M.; Bräse, S.; Baumann, T. From Iridium and Platinum to Copper and Carbon: New Avenues for More Sustainability in Organic Light-Emitting Diodes. *Green Chem.* **2015**, *17*, 1988–2011. (b) Bizzarri, C.; Spuling, E.; Knoll, D. M.; Volz, D.: Bräse, S. Sustainable Metal Complexes for Organic Light-Emitting Diodes (OLEDs). *Coord. Chem. Rev.* **2018**. *373*, 49–83.

(8) Recent review: Larsen, C. B.; Wenger, O. S. Photoredox Catalysis with Metal Complexes Made from Earth-Abundant Elements. *Chem. Eur. J*. **2018**, *24*, 2039–2058.

(9) (a) Collins, S. K.; Minozzi, C.; Caron, A.; Santandrea, J.; Grenier-Petel, J.-C. Heteroleptic Copper(I)-Based Complexes for Photocatalysis: Combinatorial Assembly, Discovery, and Optimization. *Angew. Chem., Int. Ed.* **2018**, *57*, 5477–5481. Selected reviews: (b) Reiser, O. Shining Light on Copper: Unique Opportunities for Visible-Light-Catalyzed Atom Transfer Radical Addition Reactions and Related Processes. *Acc. Chem. Res.* **2016**, *49*, 1990–1996. (c) Hernandez-Perez, A. C.; Collins, S. K. Heteroleptic Cu-Based Sensitizers in Photoredox Catalysis. *Acc. Chem. Res.* **2016**, *49*, 1557–1565.

(10) (a) Stevenson, S. M.; Higgins, R. F.; Shores, M. P.; Ferreira, E. M. Chromium Photocatalysis: Accessing Structural Complements to Diels–Alder Adducts with Electron-deficient Dienophiles. *Chem. Sci.* **2017**, *8*, 654–660. Review: (b) Büld, L. A.; Wenger, O. S. Chromium complexes for luminescence, solar cells, photoredox catalysis, upconversion, and phototriggered NO release. *Chem. Sci.* **2017**, *8*, 7359–7367.

(11) (a) Gualandi, A.; Marchini, M.; Mengozzi, L.; Natali, M.; Lucarini, M.; Ceroni, P.; Cozzi, P. G. Organocatalytic Enantioselective Alkylation of Aldehydes with $[Fe(bpy)_3]Br_2$ Catalyst and Visible Light. *ACS Catal.* **2015**, *5*, 5927–5931. Review: (b) Liu, Y.; Persson, P.; Sundström, V.; Wärnmark, K. Fe N-Heterocyclic Carbene Complexes as Promising Photosensitizers. *Acc. Chem. Res.* **2016**, *49*, 1477–1485.

(12) (a) Shields, B. J.; Kudisch, B.; Scholes, G. D.; Doyle, A. G. Long-Lived Charge-Transfer States of Nickel(II) Aryl Halide Complexes Facilitate Bimolecular Photoinduced Electron Transfer. *J. Am. Chem. Soc*. **2018**, *140*, 3035–3039. (b) Malzkuhn, S.; Wenger, O. S. Luminescent Ni(0) complexes. *Coord. Chem. Rev.* **2018**. *359*, 52–56.

(13) For selected examples of visible light photocatalysis with earth-abundant Cerium as redox active lanthanide, see: (a) Hu, A.; Guo, J.-J.; Pan, H.; Tang, H.; Gao, Z. Zuo, Z. *J. Am. Chem. Soc*. δ-Selective Functionalization of Alkanols Enabled by Visible-Light-Induced Ligand-to-Metal Charge Transfer *J. Am. Chem. Soc*. **2018**, *140*, 1612–1616. (b) Qiao, Y.; Yang, Q.; Schelter, E. Photoinduced Miyaura Borylation by a Rare Earth Photoreductant: the Hexachlorocerate(III) Anion, *Angew. Chem., Int. Ed.* **2018**, *57*, 10999–11003.

(14) Joshi-Pangu, A.; Roth, H. G.; Oliver, S. F.; Campeau, L.-C.; Nicewicz, D.; DiRocco, D. A. Acridinium-Based Photocatalysts: A Sustainable Option in Photoredox Catalysis, *J. Org. Chem*. **2016**, *81*, 7244–7249.

(15) Selected reviews: (a) Ravelli, D.; Fagnoni, M.; Albini, A. Photoorganocatalysis. What For? *Chem. Soc. Rev.* **201**3, *42*, 97–113. (b) Zeitler, K. Metal-free Photo(redox) Catalysis. in *Visible Light Photocatalysis in Organic Chemistry*; Stephenson, C. R. J.; Yoon, T. P.; MacMillan, D. W. C., Eds.; Wiley-VCH: Weinheim, 2018.

(16) (a) Arias-Rotondo, D. M.; McCusker, J. K The Photophysics of Photoredox Catalysis: a Roadmap for Catalyst Design. *Chem. Soc. Rev.* **2016**, *45*, 5803–5820. (b) Ischay, M. A.; Amenta, M. S.; Yoon, T. P. Crossed Intermolecular [2 + 2] Cycloaddition of Styrenes by Visible Light Photocatalysis. *Chem. Sci.* **2012**, ***3***, 2807–2811. (c) Singh, A.; Teegardin, K.; Kelly, M.; Prasad, K. S.; Krishnan, S.; Weaver, J. D. Facile synthesis and complete characterization of homoleptic and heteroleptic cyclometalated Iridium(III) complexes for photocatalysis *J. Organomet. Chem.,* **2015**, *776*, 51–59. (d) For ligand variations of *fac*-$Irppy_3$, see: Nacsa, E. D., MacMillan, D. W. C. Spin-Center Shift-Enabled Direct Enantioselective α-Benzylation of Aldehydes with Alcohols. *J. Am. Chem. Soc.* **2018**, *140*, 3322–3330.

(17) (a) Neumann, M.; Füldner, S.; König, B.; Zeitler, K. Metal - Free, Cooperative Asymmetric Organophotoredox Catalysis with Visible Light. *Angew. Chem. Int. Ed.* **2011**, *50*, 951–954. Review: (b) Hari, D. P.; König, B. Synthetic applications of eosin Y in photoredox catalysis. *Chem. Commun*. **2014**, *50*, 6688–6699.

(18) Fukuzumi, S.; Kotani, H.; Ohkubo, K.; Ogo, S.; Tkachenko, N. V.; Lemmetyinen, H. Electron-Transfer State of 9-Mesityl-10-methylacridinium Ion with a Much Longer Lifetime and Higher Energy Than That of the Natural Photosynthetic Reaction Center. *J. Am. Chem. Soc*. **2004**, *126*, 1600–1601.

(19) (a) Theriot, J. C.; Lim, C.-H.; Yang, H.; Ryan, M. D.; Musgrave, C. B.; Miyake, G. M. Organocatalyzed Atom Transfer

Radical Polymerization Driven by Visible Light. *Science* **2016**, *352*, 1082– 1086. (b) Poelma, S. O.; Burnett, G. L.; Discekici, E. H.; Mattson, K. M.; Treat, N. J.; Luo, Y.; Hudson, Z. M.; Shankel, S. L.; Clark, P. G.; Kramer, J. W.; Hawker, C. J.; Read de Alaniz, J. Chemoselective Radical Dehalogenation and C–C Bond Formation on Aryl Halide Substrates Using Organic Photoredox Catalysts. *J. Org. Chem.* **2016**, *81*, 7155–7160. (c) Du, Y.; Pearson, R. M.; Lim, C. H.; Sartor, S. M.; Ryan, M. D.; Yang, H.; Damrauer, N. H.; Miyake, G. M. Strongly Reducing Visible Light Organic Photoredox Catalysts as Sustainable Alternatives to Precious Metals. *Chem. Eur. J.* **2017**, *23*, 10962–10968. For a very recent study in tailoring phenoxazines as reducing photoredox catalysts, see: (d) McCarthy, B. G.; Pearson, R. M.; Lim, C.-H.; Sartor, S. M.; Damrauer, N. H.; Miyake, G. M. Structure–Property Relationships for Tailoring Phenoxazines as Reducing Photoredox Catalysts. *J. Am. Chem. Soc.* **2018**, *140*, 5088–5101.

(20) Rybicka-Jasinska, K.; Shan, W.; Zawada, K.; Kadish, K. M.; Gryko, D. Porphyrins as Photoredox Catalysts: Experimental and Theoretical Studies *J. Am. Chem. Soc.* **2016**, *138*, 15451–15458.

(21) (a) Martiny, M.; Steckhan, E.; Esch, T. Cycloaddition Reactions Initiated by Photochemically Excited Pyrylium Salts. *Chem. Ber.* **1993**, *126*, 1671–1682. (b) Miranda, M. A.; Garcia, H. 2,4,6-Triphenylpyrylium Tetrafluoroborate as an Electron-Transfer Photosensitizer. *Chem. Rev.* **1994**, *94*, 1063–1089. (c) Alfonzo, E.; Alfonso, F. S.; Beeler, A. B. Redesign of a Pyrylium Photoredox Catalyst and Its Application to the Generation of Carbonyl Ylides. *Org. Lett.* **2017**, *19*, 2989–2992. (d) Wang, K.; Meng, L.-G.; Wang, L. Visible-Light-Promoted [2 + 2 + 2] Cyclization of Alkynes with Nitriles to Pyridines Using Pyrylium Salts as Photoredox Catalysts. *Org. Lett.* **2017**, *19*, 1958–1961.

(22) For a seminal example of the employment of TADF materials in photocatalysis, see: Luo, J.; Zhang, J. Donor–Acceptor Fluorophores for Visible-Light-Promoted Organic Synthesis: Photoredox/Ni Dual Catalytic C(sp3)–C(sp2) Cross-Coupling. *ACS Catal.* **2016**, *6*, 873–877.

(23) (a) Uoyama, H.; Goushi, K.; Shizu, K.; Nomura, H.; Adachi, C. Highly efficient organic light-emitting diodes from delayed fluorescence. *Nature*, **2012**, *492*, 234–238. For review articles on organic TADF materials for OLEDs see also: (b) Yang, Z.; Mao, Z.; Xie, Z.; Zhang, Y.; Liu, S.; Zhao, J.; Xu, J.; Chi, Z.; Aldred, M. P. Recent advances in organic thermally activated delayed fluorescence materials. *Chem. Soc. Rev.* **2017**, *46*, 915–1016. (c) Wong, M. Y.; Zysman-Colman, E. Purely Organic Thermally Activated Delayed Fluorescence Materials for Organic Light‐Emitting Diodes. *Adv. Mater.* **2017**, 1605444.

(24) (a) Nishimoto, T.; Yasuda, T.; Lee, S. Y.; Kondo, R.; Adachi, C. A six-carbazole-decorated cyclophosphazene as a host with high triplet energy to realize efficient delayed-fluorescence OLEDs. *Mater. Horiz.* **2014,** 1**,** 264–269. (b) Cho, Y. J.; Jeon, S. K.; Chin, B. D.; Yu, E.; Lee, J. Y. The Design of Dual Emitting Cores for Green Thermally Activated Delayed Fluorescent Materials. *Angew. Chem., Int. Ed.* **2015**, *54*, 5201–5204. (c) Cao, X.; Zhang, D.; Zhang, S.; Tao, A.; Huang, W. CN-Containing donor–acceptor-type small-molecule materials for thermally activated delayed fluorescence OLEDs. *J. Mater. Chem. C* **2017**, *5*, 7699–7714.

(25) McNaught, A.; Wilkinson, A. Gibbs Energy of Photoinduced Electron Transfer. In IUPAC Compendium of Chemical Terminology, 2nd ed. (the "Gold Book"); Nič, M., Jirát, J., Košata, B., Jenkins, A., Eds.; Blackwell Scientific Publications: Oxford, 1997.

(26) The electronegativity of cyano groups is similar to CF_3 and CCl_3 groups and halogens (EN_{CN} = 3.3; EN_{CF3} = 3.0; EN_{CCl3} = 3.4; EN_F = 4.0; EN_{Cl} = 3.0 – Pauling Scale): Wells, P. R. Group Electronegativities. *Prog. Phys. Org. Chem.* **1968**, *6*, 111–145.

(27) For an overview on the corresponding catalyst structures including names, please see Fig. 4. Additionally, all abbreviations are summarized at the end of this article.

(28) For details and experimental proof for our revised catalyst structure **3DPAFIPN**, please see supporting information.

(29) For a selection of recent applications, see: (a) Huang, H.; Yu, C.; Zhang, Y.; Zhang, Y.; Mariano, P. S.; Wang, W. Chemo- and Regioselective Organo-Photoredox Catalyzed Hydroformylation of Styrenes via a Radical Pathway. *J. Am. Chem. Soc.* **2017**, *139*, 9799–9802. (b) Matsui, J. K.; Primer, D. N.; Molander, G. A. Metal-free C–H alkylation of heteroarenes with alkyltrifluoroborates: a general protocol for 1°, 2° and 3° alkylation. *Chem. Sci.* **2017**, *8*, 3512−3522. (c) Stache, E. E.; Rovis, T.; Doyle, A. G. Dual Nickel- and Photoredox-Catalyzed Enantioselective Desymmetrization of Cyclic meso-Anhydrides. *Angew. Chem. Int. Ed.* **2017**, *56*, 3679–3683. (d) Lévêque, C.; Chenneberg, L.; Corcé, V.; Ollivier, C.; Fensterbank, L. Organic photoredox catalysis for the oxidation of silicates: applications in radical synthesis and dual catalysis. *Chem. Commun.* **2016**, *52*, 9877–9880. (e) Loh, Y.Y.; Nagao, K.; Hoover, A. J; Hesk, D.; Rivera, N. R.; Colletti, S. L.; Davies, I. W.; MacMillan, D. W. C. Photoredox-catalyzed deuteration and tritiation of pharmaceutical compounds. *Science* **2017**, *358*, 1182−1187. (f) Meng, Q.-Y.; Wang, S.; Huff, G. S.; König, B. Ligand-Controlled Regioselective Hydrocarboxylation of Styrenes with CO_2 by Combining Visible Light and Nickel Catalysis. *J. Am. Chem. Soc.* **2018**, *140*, 3198−3201. (g) Dumoulin, A.; Matsui, J. K.; Gutiérrez-Bonet, A.; Molander, G. A. Synthesis of Non-Classical Arylated C-Saccharides through Nickel/Photoredox Dual Catalysis. *Angew. Chem., Int. Ed.* **2018**, *57*, 6614−6618. (h) Sherwood, T. C; Li, N.; Yazdani, A. N.; Dhar, T. G. M. Organocatalyzed, Visible-Light Photoredox-Mediated, One-Pot Minisci Reaction Using Carboxylic Acids via *N*-(Acyloxy)phthalimides. *J. Org. Chem.* **2018**, *83*, 3000−3012. (i) Morcillo, S. P.; Dauncey, E. M.; Kim, J. H.; Douglas, J. J.; Sheikh, N. S.; Leonori, D. Photoinduced Remote Functionalization of Amides and Amines Using Electrophilic Nitrogen‐Radicals. *Angew. Chem. Int. Ed.* **2018**, *57*, 12945−12949.

(30) Im, Y.; Kim, M.; Cho, Y. J.; Seo, J.-A.; Yook, K. S.; Lee, J. Y. Molecular Design Strategy of Organic Thermally Activated Delayed Fluorescence Emitters. *Chem. Mater.* **2017**, *29*, 1946−1963.

(31) For details on the S_NAr-type synthesis of the particular photocatalysts, please see Supporting Info.

(32) Hansch,C.; Leo, A.; Taft, R. W. A survey of Hammett substituent constants and resonance and field parameters. *Chem. Rev.* **1991**, 91, 165–195. (σ_R values: F: -0.39; Cl: -0.19; Br: -0.22; CN: +0.15). Within in the halogens only fluorine has a negative σ^+ (electron-donating/stabilizing cations) – values for σ_{para}/σ^+ F: +0.15/-0.07; Cl: +0.24/+0.11; Br: +0.26/+0.15; CN: +0.70/–). Ritchie, C. D.; Sager, W. F. An Examination of Structure-Reactivity Relationships. *Prog. Phys. Org. Chem.* **1964**, *2*, 323–400.

(33) For a correlation of the Ir^{IV}/Ir^{III} oxidation potentials of *fac*-tris-cyclometalated Ir(III) complexes with Hammett constants, see: (a) Flamigni, L.; Barbieri, A.; Sabatini, C.; Ventura, B.; Barigelletti; F. Photochemistry and Photophysics of Coordination Compounds: Iridium. *Top. Curr. Chem.* **2007**, *281*, 143–203. (b) Dedeian, K.; Djurovich, P. I.; Garces, F. O.; Carlson, G.; Watts, R. J. A new synthetic route to the preparation of a series of strong photoreducing agents: *fac*-tris-ortho-metalated complexes of iridium(III) with substituted 2-phenylpyridines. *Inorg. Chem.* **1991**, *30*, 1685−1687.

(34) Further selected examples of correlation of redox potentials with substituent effects according to Hammett constants; notably these correlations are typically only applied for *oxidation* potentials only, : (a) Jovanovic, S. V.; Tosic, J. M.; Simic, M. G. Use of the Hammett Correlation and σ^+ for Calculation of One-Electron Redox Potentials of Antioxidants. *J. Phys. Chem.* **1991**, *95,* 10824–10827. (b) Silva, M. E. N. P. R. A.; Pombeiro, A. J. L.; da Silva, J. J. R. F.; Herrmann, R.; Deus, Castilho, N.;T. J; Silva, M. F. C. G. Redox potential and substituent effects at ferrocene

derivatives. Estimates of Hammett σ_p and Taft polar σ^* substituent constants. *J. Organomet.* **1991**, *421*, 75–90. (c) Dapperheld, S.; Steckhan, E.; Grosse Brinkhaus, K. H.; Esch. T. Substituted Triarylamine Cation-Radical Redox Systems - Synthesis, Electrochemical and Spectroscopic Properties, Hammett Behavior, and Suitability as Redox Catalysts. *Chem. Ber.* **1991**, *124*, 2557–2567. (d) Zhang, N.-T.; Zeng, C.-C.; Lam, C. M.; Gbur, R. K.; Little, R. D. Triarylimidazole Redox Catalysts: Electrochemical Analysis and Empirical Correlations. *J. Org. Chem.* **2013**, *78*, 2104– 2110. (e) Francke, R.; Little, R. D. Optimizing Electron Transfer Mediators Based on Arylimidazoles by Ring Fusion: Synthesis, Electrochemistry, and Computational Analysis of 2-Aryl-1-methylphenanthro[9,10-*d*]imidazoles. *J. Am. Chem. Soc.* **2014**, *136*, 427–435.

(35) (a) Wang, J.; Sánchez-Roselló, M.; Aceña, J. L.; del Pozo, C.; Sorochinsky, A. E.; Fustero, S.; Soloshonok, V. A.; Liu, H. Fluorine in pharmaceutical industry: fluorine-containing drugs introduced to the market in the last decade (2001–2011). *Chem. Rev.* **2014**, *114*, 2432–2506. (b) Meanwell, N. A. Fluorine and Fluorinated Motifs in the Design and Application of Bioisosteres for Drug Design. *J. Med. Chem.* **2018**, *61*, 5822–5880 and references cited therein.

(36) (a) Cho, Y. J.; Chin, B. D.; Jeon, S. K.; Lee, J. Y. 20% External Quantum Efficiency in Solution-Processed Blue Thermally Activated Delayed Fluorescent Devices. *Adv. Funct. Mater.* **2015**, *25*, 6786–6792. (b) Zhang, J.; Li, J.; Chen, W.; Zheng, D.; Yu, J.; Wang, H.; Xu, B. An Efficient Blue Thermally Activated Delayed Fluorescence Material Based on 4-Fluorocyanobenzene Derivative for Organic Light-emitting Diodes. *Tetrahedron Lett.* **2016**, *57*, 2044–2048.

(37) For a recent study of attaching halogen atoms (Cl, Br, I) to the donor carbazoles of **4CzIPN** as TADF emitter and their effect on decreasing the half-life of the delayed fluorescence avoiding emitter degradation, see: (a) Kretzschmar, A.; Patze, C.; Schwaebel, T.; Bunz, U. H. F. Development of Thermally Activated Delayed Fluorescence Materials with Shortened Emissive Lifetimes. *J. Org. Chem.* **2015**, *80*, 9126–9131. For a recent example of using similar structures as photocatalysts: (b) Le Vaillant, F.; Garreau, M.; Nicolai, S.; Gryn'ova, G.; Corminboeuf, C.; Waser, J. Fine-tuned organic photoredox catalysts for fragmentation-alkynylation cascades of cyclic oxime ethers. *Chem. Sci.* **2018**, *9*, 5883–5889.

(38) Adachi, C.; Uoyama, H.; Nomura, H.; Goushi, K.; Yasuda, T.; Kondo, R.; Shizu, K.; Nakanotani, H.; Nishide, J. Organic light emitting element, and light emitting material and compound used in same. WO2013154064 A1, 2013–10–17.

(39) Zhang, D.; Cai, M.; Zhang, Y.; Zhang, D.; Duan, L. Sterically shielded blue thermally activated delayed fluorescence emitters with improved efficiency and stability. *Mater. Horiz.* **2016**, *3*, 145–151.

(40) For the redox potentials of all metal based catalysts see ref. 1c; for Eosin Y see: Hari, D. P.; König, B. Synthetic applications of eosin Y in photoredox catalysis. *Chem. Commun*. **2014**, *50*, 6688–6699. For Mes-Acr$^+$ and Mes-MeOAcr$^+$ see ref 14 (**Mes-MeOAcr$^+$** is titled as acridinium **7** in ref 14).

(41) Chu, L.; Ohta, C.; Zuo, Z.; MacMillan, D. W. C. Carboxylic Acids as A Traceless Activation Group for Conjugate Additions: A Three-Step Synthesis of (±)-Pregabalin. *J. Am. Chem. Soc.* **2014**, *136*, 10886–10889.

(42) This hypothesis is corroborated by their strikingly weak radiative emission intensity (*cf.* Supporting information: Figure SI27 in comparison to other derivatives of the series), suggesting competitive non-radiative relaxation processes to be operative as maybe triggered by **MeOCz** as stronger donor substituent. A more detailed investigation of these phenomena is currently underway. For examples of CT effects in donor-acceptor molecules, see: (a) Kosower, E. M.; Dodiuk, H.; Kanety, H. Intramolecular donor-acceptor system. 4. Solvent effects on radiative and nonradiative processes for the charge-transfer states of *N*-arylaminonaphthalenesulfonates. *J. Am. Chem. Soc*. **1978**, *100*, 4179–4188.. (b) Ishimatsu, R.; Matsunami, S.; Shizu, K.; Adachi, C.; Nakano, K.; Imato, T. Solvent Effect on Thermally Activated Delayed Fluorescence by 1,2,3,5-Tetrakis(carbazol-9-yl)-4,6-dicyanobenzene. *J. Phys. Chem. A* **2013**, *117*, 5607–5612. (c) Im, J. B.; Lampande, R.; Kim, G. H., Lee; J. Y.; Kwon, J. H. Thermally Activated Delayed Fluorescence Behavior Investigation in the Different Polarity Acceptor and Donor Molecules. *J. Phys. Chem. C* **2017**, *121*, 1305–1314.

(43) Ohkubo, K.; Mizushima, K.; Iwata, R.; Fukuzumi, S. Selective photocatalytic aerobic bromination with hydrogen bromidevia an electron-transfer state of 9-mesityl-10-methylacridinium ion. *Chem. Sci*. **2011**, *2*, 715–722.

(44) Nguyen, J. D.; Matsuura, B. S.; Stephenson, C. R. J. Photochemical Strategy for Lignin Degradation at Room Temperature. *J. Am. Chem. Soc.* **2014**, *136*, 1218–1221.

(45) Luo, J.; Zhang, X.; Lu, J.; Zhang, J. Fine Tuning the Redox Potentials of Carbazolic Porous Organic Frameworks for Visible-Light Photoredox Catalytic Degradation of Lignin β-O-4 Models. *ACS Catal*. **2017**, *7*, 5062–5070.

(46) Nakajima, M.; Fava, E.; Loeschner, S.; Jiang, Z.; Rueping, M. Photoredox‐Catalyzed Reductive Coupling of Aldehydes, Ketones, and Imines with Visible Light. *Angew. Chem. Int. Ed*. **2015**, *54*, 8828–8832.

(47) Yield of **8** could only be determined by product isolation. Quantification using GC-FID is hampered by a thermally initiated back reaction to acetophenone during heating in the GC.

(48) (a) Speckmeier, E.; Zeitler, K. Desyl and Phenacyl as Versatile, Photocatalytically Cleavable Protecting Groups: A Classic Approach in a Different (Visible) Light. *ACS Catal*. **2017**, *7*, 6821–6826. (b) Speckmeier, E.; Padié, C.; Zeitler, K. Visible Light Mediated Reductive Cleavage of C–O Bonds Accessing α-Substituted Aryl Ketones. *Org. Lett*. **2015**, *17*, 4818–4821. (c) Speckmeier, E.; Klimkait, M.; Zeitler, K. Unlocking the Potential of Phenacyl Protecting Groups: CO_2-Based Formation and Photocatalytic Release of Caged Amines. *J. Org. Chem.* **2018**, *83*, 3738–3745. (d) Speckmeier, E.; Fuchs, P. J. W.; Zeitler, K. A Synergistic LUMO Lowering Strategy Using Lewis Acid Catalysis in Water to Enable Photoredox Catalytic, Functionalizing C-C Cross-Coupling of Styrenes. *Chem. Sci.* **2018**, *9*, 7096–7103.

(49) Jutand, A.; Négri, S. Activation of Aryl and Vinyl Triflates by Palladium and Electron Transfer – Electrosynthesis of Aromatic and a,β-Unsaturated Carboxylic Acids from Carbon Dioxide. *Eur. J. Org. Chem.* **1998**, 1811–1821.

(50) (a) Ghosh, I.; Shaikh, R. S.; König, B. Sensitization‐Initiated Electron Transfer for Photoredox Catalysis. *Angew. Chem. Int. Ed*. **2017**, *56*, 8544–8549. (b) Shaikh, R. S.; Düsel, S. J. S.; König, B. Visible-Light Photo-Arbuzov Reaction of Aryl Bromides and Trialkyl Phosphites Yielding Aryl Phosphonates. *ACS Catal*. **2016**, *6*, 8410–8414.

(51) Ghosh, I.; Ghosh, T.; Bargadi, J. I.; König, B. Reduction of aryl halides by consecutive visible light-induced electron transfer processes. *Science*, **2014**, *346*, 725–728.

(52) Ghosh, I.; König, B. Chromoselective Photocatalysis: Controlled Bond Activation through Light-Color Regulation of Redox Potentials. *Angew. Chem. Int. Ed*. **2016**, *55*, 7676–7679.

(53) Majek, M.; Faltermeier, U.; Dick, B.; Perez-Ruiz, R.; Jacobi von Wangelin, A. Application of Visible‐to‐UV Photon Upconversion to Photoredox Catalysis: The Activation of Aryl Bromides. *Chem. Eur. J.* **2015**, *21*, 15496–15501.

(54) For a detailed, additional graphical representation of the course of the reaction for all tested reductive transformations, please see supporting info.

(55) Under the tested diluted conditions (c(PC) = 0.4 mM) a doubling of the catalyst loading did not prove to be beneficial; see supporting information for details.

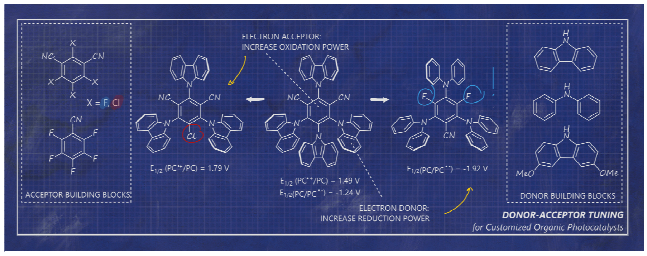
ELECTRON ACCEPTOR:
INCREASE OXIDATION POWER
X = F, Cl
ACCEPTOR BUILDING BLOCKS
$E_{1/2}(PC^{*}/PC) = 1.79$ V
$E_{1/2}(PC^{*}/PC) = 1.49$ V
$E_{1/2}(PC/PC^{\bullet-}) = -1.24$ V
$E_{1/2}(PC/PC^{\bullet-}) = -1.10$ V
ELECTRON DONOR:
INCREASE REDUCTION POWER
DONOR BUILDING BLOCKS
DONOR-ACCEPTOR TUNING
for Customized Organic Photocatalysis

...